

Journal of Materials Chemistry C

Accepted Manuscript



This article can be cited before page numbers have been issued, to do this please use: W. Cho, G. Sarada, A. Maheshwaran, Y. Gal, Y. Nam, J. Y. Lee and S. Jin, *J. Mater. Chem. C*, 2017, DOI: 10.1039/C7TC02557B.



This is an Accepted Manuscript, which has been through the Royal Society of Chemistry peer review process and has been accepted for publication.

Accepted Manuscripts are published online shortly after acceptance, before technical editing, formatting and proof reading. Using this free service, authors can make their results available to the community, in citable form, before we publish the edited article. We will replace this Accepted Manuscript with the edited and formatted Advance Article as soon as it is available.

You can find more information about Accepted Manuscripts in the [author guidelines](#).

Please note that technical editing may introduce minor changes to the text and/or graphics, which may alter content. The journal's standard [Terms & Conditions](#) and the ethical guidelines, outlined in our [author and reviewer resource centre](#), still apply. In no event shall the Royal Society of Chemistry be held responsible for any errors or omissions in this Accepted Manuscript or any consequences arising from the use of any information it contains.

Solution-Processable Highly Efficient Deep-Red and Orange Organic Light-Emitting Diodes Based on Multi-functional Ir(III) Complexes

Woosum Cho,^{‡a} Ganguri Sarada,^{‡a} Athithan Maheshwaran,^a Yeong-Soon Gal,^b Yeonsig Nam,^c Jin Yong Lee^{*c}, and Sung-Ho Jin^{*a}

^aDepartment of Chemistry Education, Graduate Department of Chemical Materials and Institute for Plastic Information and Energy Materials, Pusan National University, Busan, 46241, Republic of Korea, *E-mail: shjin@pusan.ac.kr

^aDepartment of Fire Safety, Kyungil University, Gyeongsangbuk-do 38428, Republic of Korea

^cDepartment of Chemistry, Sungkyunkwan University, Suwon 16419, Republic of Korea, *E-mail: jinylee@skku.edu

[‡] These authors contributed equally to this work

Abstract: The heteroleptic deep-red iridium(III) complex, TPQIr-HT based on thiophene-phenylquinoline (TPQ), and orange Ir(III) complexes, *m*-CF₃DPQIr-HT and *m*-CF₃DPQIr-ET based on diphenylquinoline (DPQ), were designed by attaching a carbazole-based hole transporting (HT) group and an oxadiazole (OXD)-based electron transporting (ET) group to the parent Ir(III) complexes, TPQIr and *m*-CF₃DPQIr. The Ir(III) complexes TPQIr-HT showed a deep-red emission peak at 612 nm, similar to that of TPQIr, whereas *m*-CF₃DPQIr-HT and *m*-CF₃DPQIr-ET showed an orange emission peak at 567±1 nm, which is similar to that of *m*-CF₃DPQIr. The newly functionalized Ir(III) complexes showed improved device performance compared to the Ir(III) complexes, TPQIr and *m*-CF₃DPQIr, without the additional functional groups. The phosphorescent organic light-emitting diodes (PhOLEDs) fabricated using the deep-red Ir(III) complex, TPQIr-ET, achieved a maximum external quantum efficiency (EQE) of 17.47% using GraHIL as the hole injection layer (HIL). Similarly, the orange Ir(III) complex, *m*-CF₃DPQIr-HT, achieved a maximum EQE of 21.61%.

1. Introduction

Solution-processed phosphorescent organic light-emitting diodes (PhOLEDs) have attracted great interest for cost effective and large-area manufacturing of solid-state lighting and displays sources.¹⁻⁵ Ir(III) complexes are considered most promising emitters in OLEDs due to their high quantum yields, strong spin-orbit couplings, short triplet lifetimes, and emission color tunability from blue to deep-red.^{6,7} Deep-red phosphorescent emitters and PhOLEDs with Commission International de L'Eclairage (CIE) ≥ 0.67 are still rare, despite extensive efforts applying novel dopant and host materials to attain high performance solution-processed deep-red PhOLEDs.⁸⁻¹¹ Recently, deep-red and orange PhOLEDs using Ir(III) complex emitters achieved a high external quantum efficiency (EQE) of about 26 and 28%, respectively, through vapor deposition processes.¹²⁻¹⁷ The performance of solution-processed PhOLEDs is still inferior to the vacuum-deposited counterparts in terms of efficiency, turn-on voltages (V_{on}) and efficiency roll-off at high current densities.¹⁸⁻²² Highly efficient orange phosphorescent emitters are indispensable for the fabrication of two-component white OLEDs.²³⁻²⁷

Many research groups have focused on the design and synthesis of novel solution-processable deep-red and orange emitting phosphors with different design strategies. For example, Cao et al. reported a series of Ir(III) complexes through the incorporation of hole transporting (HT) triphenylamine units and/or electron transporting (ET) phosphine oxide groups to the cyclometalating (C^N) ligand phenylisoquinoline. Among them, one phosphor (R2) showed a maximum EQE of 7.6% with CIE coordinates of (0.68, 0.30).²⁸ Xie et al. synthesized Ir(ht-5ht-py)₂(acac), by introducing hexyl side chain on the ligand to improve

miscibility with the host materials to form a homogeneous emissive layer, which exhibited a decent EQE of 8.2% with satisfactory CIE coordinates of (0.68, 0.31) for saturated red emission.²⁹

In our previous works, we reported deep-red emitting solution-processable Ir(III) complexes *o*-CF₃DPQIr_{tmd} based on diphenylquinoline (DPQ),³⁰ (FPQ)₂Ir(pic-N-O) based on fluorenyl-phenylquinoline (FPQ),³¹ and (EO-Cz-PQ)₂Ir(acac) based on carbazolyl (Cz)-phenylquinoline (PQ)³² ligands. Their PhOLEDs exhibited EQEs of 3.7, 8.9 and 4.74% with CIE coordinates of (0.663, 0.336), (0.660, 0.338) and (0.65, 0.34), respectively. We also reported a thiophene-phenylquinoline (TPQ)-based highly efficient solution-processable homoleptic Ir(III) complex, Ir(Th-PQ)₃, with deep-red CIE coordinates (0.64, 0.34).³³ Using the same C[^]N ligand (TPQ), we have also reported a deep-red emitting heteroleptic Ir(III) complex, TPQIr-ET,³⁴ by incorporating an ET functional moiety, oxadiazole (OXD) unit, onto the ancillary ligand. TPQIr-ET achieved a high EQE of 20.59% in solution-processed PhOLEDs with CIE coordinates (0.673, 0.323) due to the balanced charge carrier injection by the ET functional group. In addition, we reported the orange emitting solution-processable Ir(III) complexes *m*-CF₃DPQIr_{pic}, *p*-CF₃DPQIr_{pic} and (DPQ)₂Ir(pic-N-O) using DPQ-based C[^]N ligands and their PhOLEDs exhibited EQEs of 17.1, 12.8 and 14.2%, respectively.^{30,31}

Here, we synthesized a new deep-red heteroleptic Ir(III) complex, TPQIr-HT (Scheme 2), suitable for solution process, by incorporating an HT functional group, (9-(3-(9H-carbazol-9-yl)phenyl)-3-ethyl-9H-carbazol) (mCP), onto the ancillary ligand to facilitate charge balance in the emitting layer (EML). We also synthesized new orange emitting heteroleptic Ir(III) complexes, *m*-CF₃DPQIr-HT and *m*-CF₃DPQIr-ET (Scheme 3), for solution process by incorporating ET and HT functional groups on the ancillary ligand. The PhOLED of TPQIr-HT furnished deep-red CIE coordinates of (0.67, 0.32) and a high EQE of 17.47%. Also, the

PhOLEDs of *m*-CF₃DPQIr-HT and *m*-CF₃DPQIr-ET exhibited common orange CIE coordinates of (0.54, 0.46) and a high EQE of 21.61 and 18.39%, respectively.

2. Experimental

2.1 General information

All chemicals and reagents were purchased from Aldrich Chemical Co. and used without further purification. Compound 1, TPQIr-Cl in Scheme 2^{34,35}; compound 6, mCPCH₂Br and OXDCH₂Br in Scheme 3 were synthesized using the reported procedures.^{35,36} ¹H NMR spectra were recorded on a Varian Mercury Plus 300 MHz spectrometer in CDCl₃ using tetramethylsilane as an internal standard. Thermal gravimetric analysis (TGA) was carried out by Mettler Toledo TGA/SDTA 851e under N₂ atmosphere at a heating rate of 10 °C/min. The UV-vis absorption and the fluorescence spectra were recorded with JASCO V-570 and Hitachi F-4500 fluorescence spectrophotometers at room temperature (RT), respectively. Cyclic voltammetry (CV) measurements were performed with a CHI 600C potentiostat (CH Instruments) at a scan rate of 100 mV/s using anhydrous dichloromethane (CH₂Cl₂) and 0.1 M tetrabutylammonium tetrafluoroborate (TBABF₄) as the solvent and electrolyte, respectively, at RT. A platinum disc was used as the working electrode, a platinum wire as the counter electrode, and a Ag/AgCl as the reference electrode. The potentials were referenced to the ferrocene/ferrocenium redox couple (Fc/Fc⁺). A sublimated grade of 4,4',4''-tris(*N*-carbazolyl)-triphenylamine (TCTA), 1,3,5-tris(*N*-phenylbenzimidazole-2-yl)benzene (TPBi), 4,4'-cyclohexylidenebis[*N,N*-bis(4-methylphenyl)benzenamine] (TAPC), and 2,6-bis(3-(9*H*-Carbazol-9-yl)phenyl)pyridine (26DCzPPy) were purchased from OSM and used as the host materials for the EMLs of the orange and deep-red emitting PhOLEDs. A sublimated grade of 1,3,5-tri[(3-pyridyl)-phen-3-yl]benzene (TmPyPB) purchased from OSM was used as an ET layer (ETL). The process of fabrication and characterizations of PhOLEDs are described in

supporting information (SI).

2.2 Synthesis of 9-(3-(9H-carbazol-9-yl)phenyl)-9H-carbazole-3-carbaldehyde (2).

Phosphoryl chloride (200 mmol) was added dropwise into N,N-dimethylformamide (DMF, 200 mmol) in an ice bath. The mixture was stirred at RT for 1 h and a solution of 1,3-di(9H-carbazol-9-yl)benzene (**1**, 3.27 g, 8 mmol) in 10 mL of DMF was added. The reaction mixture was heated at 130 °C with stirring for 24 h and then poured into ice water. After neutralizing with a base, the mixture was extracted with chloroform (CHCl₃). The organic layer was dried over anhydrous Na₂SO₄ and the solvent was removed by distillation under vacuum. The solid residue was purified by column chromatography on silica gel (hexane:ethyl acetate (EtOAc), 4:1 v/v) to obtain a whitish-yellow solid, **2** (1.92 g, 55%). ¹H NMR (300 MHz, CDCl₃): δ (ppm) 10.13 (s, 1H), 8.69 (s, 1H), 8.24-8.21 (d, 1H), 8.17-8.15 (d, 2H), 8.00-7.98 (d, 1H), 7.90-7.87 (m, 1H), 7.80 (m, 2H), 7.70-7.68 (d, 2H), 7.60-7.56 (m, 4H), 7.47-7.42 (m, 3H), 7.35-7.30 (t, 2H).

2.3 Synthesis of (9-(3-(9H-carbazol-9-yl)-9H-carbazol-3-yl)methanol (mCPCH₂OH).

To a solution of compound **2** (1.92 g 4.34 mmol) in ethanol (40 mL) and CH₂Cl₂ (40 mL), NaBH₄ was added slowly at RT. The reaction mixture was stirred for 3 h at RT and then poured into water (70 mL) and extracted with CH₂Cl₂. The organic layer was washed with water, dried over Na₂SO₄ and concentrated under vacuum to get the crude product. The desired product, mCPCH₂OH, was obtained as a colorless solid (1.8 g, 94%) upon recrystallization in toluene. ¹H NMR (300 MHz, CDCl₃): δ (ppm) 8.15 (s, 4H), 7.85-7.78 (m, 2H), 7.70-7.69 (m, 2H), 7.53-7.44 (m, 8H), 7.34-7.26 (m, 3H), 4.88 (d, 2H), 1.78 (s, 1H).

2.4 Synthesis of bis[4-phenyl-2-(thiophen-2-yl)quinoline]iridium (9-(3-(9H-carbazol-9-yl)-9H-carbazol-3-yl) piconlinate (TPQIr-HT).

A mixture of TPQIr-Cl (1.50 g, 1.63 mmol), mCPCH₂OH (1.07 g, 2.45 mmol), and K₂CO₃

(2.18 g, 16.3 mmol) in DMF (20 mL) was stirred at 80 °C under N₂ atmosphere for 12 h. The resulting mixture was cooled to RT followed by the addition of cold water and further extracted with CH₂Cl₂. The organic layer was dried over anhydrous Na₂SO₄ and then the solvent was evaporated under reduced pressure. The solid crude product was purified by column chromatography on silica gel (EtOAc:CH₂Cl₂:hexane, 3:5:2 v/v/v) to furnish a red powder, TPQIr-HT (0.78 g, 36%). ¹H NMR (300 MHz, CDCl₃): δ (ppm) 8.15 (s, 4H), 7.85-7.78 (m, 2H), 7.70-7.69 (m, 2H), 7.53-7.44 (m, 8H), 7.34-7.26 (m, 3H), 4.88 (s, 2H), 1.78 (s, 1H). Anal. calcd for C₇₅H₄₈IrN₅O₃S₂: C, 68.06; H, 3.66; N, 5.29; found C, 67.91; H, 3.60; N, 5.23.

2.5 Synthesis of bi[4-phenyl-2-(3-(trifluoromethyl)phenyl)quinoline]iridium piconlinate hydroxyl (*m*-CF₃DPQIr-OH) (7).

The dimer (2 g, 1.08 mmol) and 3-hydroxypicolinic acid (0.752 g, 5.41 mmol) were mixed with Na₂CO₃ (1.14 g, 10.92 mmol) in 2-ethoxyethanol (50 mL). The mixture was stirred for 12 h at RT under N₂ atmosphere. After completion of the reaction, the mixture was poured into water and extracted with CH₂Cl₂, dried over anhydrous Na₂SO₄ and the solvent was evaporated under vacuum. The residue was then purified by column chromatography on silica gel (hexane:EtOAc, 6:4 v/v) to furnish compound *m*-CF₃DPQIr-OH (7) as a dark orange solid (0.66 g, 60%). ¹H NMR (300 MHz, CDCl₃): δ (ppm) 13.28 (s, 1H), 8.70-8.67 (d, J=9.3 Hz, 1H), 8.16 (s, 1H), 8.08 (m, 3H), 7.89-7.86 (d, J=7.5 Hz, 2H), 7.63 (s, 11H), 7.48-7.34 (m, 4H), 7.26-7.22 (m, 2H), 7.03-7.01 (m, 3H), 6.93-6.90 (d, J=8.7 Hz, 1H), 6.50-6.47 (d, 1H).

2.6 Synthesis of bi[4-phenyl-2-(3-(trifluoromethyl)phenyl)quinoline]iridium (9-(3-(9H-carbazol-9-yl)-9H-carbazol-3-yl) piconlinate (*m*-CF₃DPQIr-HT).

A mixture of *m*-CF₃DPQIr-OH (0.5 g, 0.486 mmol), mCPCH₂Br and Cs₂CO₃ (0.32 g,

0.973 mmol) in acetone (25 mL) was refluxed for 8 h under N₂ atmosphere. After cooling to RT, the solvent was evaporated and the residue was dissolved in CH₂Cl₂. The organic phase was washed with water, dried with Na₂SO₄ and purified using flash chromatography on silica gel (hexane:EtOAc, 3:2 v/v) to afford *m*-CF₃DPQIr-HT as a dark orange solid (0.42 g, 60%). ¹H NMR (300 MHz, CDCl₃): δ (ppm) 8.99-8.96 (d, J=8.7 Hz, 1H), 8.17-8.08 (q, J=27 Hz, 6H), 8.03-8.01 (d, J=6 Hz, 2H), 7.78-7.70 (m, 3H), 7.66-7.58 (m, 15H), 7.45-7.36 (m, 10H), 7.30-7.28 (m, 5H), 7.05-6.96 (q, J=26.4 Hz, 2H), 6.88-6.86 (d, J=6.9 Hz, 1H), 6.80-6.75 (t, J=14.7 Hz, 1H), 6.65-6.60 (t, J=14.7 Hz, 1H), 6.41-6.39 (d, J=7.8 Hz, 1H), 5.22 (s, 2H). Anal. calcd for C₈₁H₅₀F₆IrN₅O₃: C, 67.21; H, 3.48; N, 4.84; found C, 67.30; H, 3.42; N, 4.79.

2.7 Synthesis of bi[4-phenyl-2-(3-(trifluoromethyl)phenyl)quinoline]iridium 4-(4-(5-phenyl-1,3,4-oxadiazol-2-yl)phenoxy)picolinate (*m*-CF₃DPQIr-ET).

A mixture of *m*-CF₃DPQIr-OH (0.5 g, 0.486 mmol), OXDCH₂Br, and Cs₂CO₃ (0.32 g, 0.973mmol) in acetone (25 mL) was refluxed for 8 h under N₂ atmosphere. After cooling to RT, the solvent was evaporated and the residue was dissolved in CH₂Cl₂. The organic phase was washed with water, dried over Na₂SO₄ and purified using flash chromatography on silica gel (hexane:EtOAc, 4:2 v/v) to afford *m*-CF₃DPQIr-ET as an orange solid (0.43 g, 70%). ¹H NMR (300 MHz, CDCl₃): δ (ppm) 9.02-8.99 (d, J=9.3 Hz, 1H), 8.16-8.01 (m, 8H), 7.92-7.89 (t, J =17.4 Hz, 2H), 7.67-7.55 (m, 16H), 7.41-7.48 (m, 4H), 7.19 (m, 2H), 7.05-7.00 (q, 2H), 6.91 (m, 2H), 6.45-6.42 (d, J=9 Hz, 1H), 5.18 (s, 2H). Anal. calcd for C₆₅H₄₀F₆IrN₅O₄: C, 61.90; H, 3.20; N, 5.55; found C, 61.81; H, 3.16; N, 5.63.

3. Results and discussion

The three Ir(III) complexes, TPQIr-HT, *m*-CF₃DPQIr-HT and *m*-CF₃DPQIr-ET, were successfully synthesized according to the routes shown in Schemes 2 and 3. The molecular

structures were thoroughly characterized by ^1H NMR spectroscopy and elemental analysis. TPQIr-HT, *m*-CF₃DPQIr-HT and *m*-CF₃DPQIr-ET showed moderate thermal stability with decomposition temperatures ($\Delta T_{5\%}$, corresponding to 5% weight loss) comparable to those of TPQIr and *m*-CF₃DPQIr (Fig. S1). As shown in Fig. 1, UV-vis absorption and photoluminance (PL) spectra of TPQIr, TPQIr-HT, TPQIr-ET, *m*-CF₃DPQIr, *m*-CF₃DPQIr-HT and *m*-CF₃DPQIr-ET measured at RT in CHCl₃ solution (10⁻⁵ M) and in film state, resemble the UV-vis absorption and PL spectrum of the parent Ir(III) complexes, TPQIr and *m*-CF₃DPQIr. The introduction of mCP and OXD groups on picolinic acid did not affect the ground or emissive excited state energies of the Ir(III) complexes. The strong absorption peaks at 300 and 350 nm can be assigned to the spin-allowed $^1\pi-\pi^*$ bands of the C^N ligands. The low-energy broad bands between 430 and 560 nm were attributed to the metal-to-ligand charge transfer excitations, $^1\text{MLCT}$ and $^3\text{MLCT}$, representing the strong spin-orbit coupling effects induced by the heavy metal center. Upon irradiation, TPQIr-HT emitted bright red light at the maximum PL (PL_{max}) of 612 nm, which was slightly red shifted from TPQIr and TPQIr-ET (Fig. 1a). Also *m*-CF₃DPQIr-HT and *m*-CF₃DPQIr-ET emitted bright orange light at the PL_{max} of 567-568 nm, which was slightly red shifted from *m*-CF₃DPQIr (Fig. 1b). Thermal, photophysical and electrochemical properties of the new Ir(III) complexes are presented in Table 1.

The PL quantum yield (Φ_{PL}) of TPQIr-HT, *m*-CF₃DPQIr-HT and *m*-CF₃DPQIr-ET were measured in degassed CHCl₃ solution at RT using Ir(pic)₂(acac) ($\Phi_{\text{PL}} = 0.20$ in CHCl₃) as standard. TPQIr-HT exhibited Φ_{PL} of 0.20, compared to 0.68 and 0.66 for *m*-CF₃DPQIr-HT and *m*-CF₃DPQIr-ET, respectively. CV analysis was carried out for TPQIr-HT, *m*-CF₃DPQIr-HT and *m*-CF₃DPQIr-ET to find the highest occupied molecular orbital (HOMO) energy level and the lowest unoccupied molecular orbital (LUMO) energy level. The experimental

HOMO energies were -5.24, -5.41 and -5.42 eV and the LUMO were -3.29, -3.11 and -3.10 eV for TPQIr-HT, *m*-CF₃DPQIr-HT and *m*-CF₃DPQIr-ET (Fig. S2), respectively. Both the HOMO and LUMO levels of TPQIr-HT were very close to the corresponding energy levels of TPQIr and TPQIr-ET.³⁴ HOMO and LUMO of *m*-CF₃DPQIr-HT and *m*-CF₃DPQIr-ET were almost the same as the corresponding energy levels of *m*-CF₃DPQIr³⁰, indicating that the introduction of either an carbazole-based HT or OXD-based ET group on the ancillary ligand did not greatly influence the frontier orbital energy levels of these Ir(III) complexes, similar to their photophysical properties.

The density functional theory (DFT) analysis for Ir(III) complexes was performed with the suite of Gaussian09 programs using B3LYP functional with 6-31G(d) basis set for C, H, N, O, F, and S, and LANL2DZ for Ir atom.³⁷ The HOMO electron density of TPQIr-HT was majorly distributed over the Ir(III) metal and on the thiophene-quinoline rings of TPQ, while the LUMO was located on the phenylquinoline of TPQ (Fig. S3). This shows that MLCT probably contributed to the transition properties. To clearly understand the spatial distribution of the frontier molecular orbitals, the contour plots of HOMO to HOMO-2 and LUMO to LUMO+2 of *m*-CF₃DPQIr, *m*-CF₃DPQIr-HT and *m*-CF₃DPQIr-ET are given in Fig. S4, Fig. S5 and Fig. S6, respectively, and the calculated energies are summarized in Table S1. In general, for the three orange Ir(III) complexes, the LUMOs were mainly located on picolinic acid and the *m*-CF₃DPQ main ligand. The HOMOs and HOMO-1 of *m*-CF₃DPQIr and *m*-CF₃DPQIr-ET were located largely on the metal center and the -CF₃ substituted phenyl ring of the cyclometalating ligands. Conversely, the HOMO and HOMO-1 of *m*-CF₃DPQIr-HT were located entirely on mCP, which reveals the intramolecular energy transfer from mCP to the Ir(III) complex unit.^{33,36} Noticeably, the metal atom contributed HOMO and HOMO-1 for *m*-CF₃DPQIr and *m*-CF₃DPQIr-ET (Fig. 4 and 6), whereas it contributed HOMO-2 for *m*-

CF₃DPQIr-HT. Hence, this in depth analysis of the molecular orbitals (HOMO to HOMO-2 and LUMO to LUMO+2) implies the MLCT character of the transitions.

The electron and hole mobilities of TPQIr-HT were measured by using the space-charge limited current (SCLC)³⁹ method with a device configuration of ITO/LiF (10 nm)/Ir(III) complex (100 nm)/LiF (1 nm)/Al (100 nm) for the electron-only device and an ITO/PEDOT:PSS (40 nm)/Ir(III) complex (100 nm)/MoO₃ (5 nm)/Al (100 nm) for the hole-only device. The electron and hole mobilities of TPQIr and TPQIr-ET were also measured by the same method (Table S2). The current density versus voltage ($J-V^2$) plots for the devices are shown in Fig. S7. The electron and hole mobilities of TPQIr-HT were 8.72×10^{-5} and 2.84×10^{-4} cm²/V s, respectively. This result clearly shows that tethering an mCP unit to the Ir(III) complex not only improved the hole mobility but also the electron mobility, as compared with TPQIr. The mobility results of *m*-CF₃DPQIr-HT and *m*-CF₃DPQIr-ET also followed the same trend of TPQIr-HT and TPQIr-ET, i.e., the electron and hole mobilities of *m*-CF₃DPQIr-HT and *m*-CF₃DPQIr-ET were 3.22×10^{-5} and 6.02×10^{-4} cm²/V s and 4.73×10^{-4} and 8.32×10^{-5} cm²/V s, respectively. S. -W. Lin et al. reported that hole and electron mobilities of mCP are in the order of 10^{-4} cm²/V s and also reported that mCP's hole mobility is higher than electron mobility.⁴⁰ However, the carrier mobilities of TPQIr and *m*-CF₃DPQIr is lower compared to mCP. Thus by the attachment of mCP-based HT unit, the carrier mobilities of both electron and hole is improved.

In order to evaluate the PhOLEDs performance of TPQIr-HT as an emitter, we fabricated deep-red PhOLEDs with a simple device structure containing a solution-processed hole injection layer (HIL) and EML (Fig. 2a). The device configuration adopted in this study was an ITO/GraHIL/TCTA:TPBi:Ir(III) complex (10 wt %)/TmPyPB/LiF/Al, where TCTA:TPBi acts as the mixed cohost for the EML. Here, GraHIL, a self-organized polymeric gradient

HIL, composed of PEDOT:PSS and a perfluorinated oligomer with a low surface energy tetrafluorethylene-perfluoro-3,6-dioxo-4-methyl-7-octene-sulfonic acid oligomer (PFI) in 2:1 weight ratio,⁴¹⁻⁴³ was used as HIL. GraHIL has a gradient work function, which gradually increases from ~4.8 to ~5.63 eV due to the self-organization of PFI. This phenomenon is very important to realize an efficient hole injection into the EML by reducing the injection barrier at the HIL/EML interface.⁴¹ Therefore, the deep-red PhOLEDs do not require an additional layer for hole injection between HIL and EML. TmPyPB was used as ETL. We also fabricated control devices using TPQIr and TPQIr-ET as dopants to compare the effect of the mCP group on the device performance.

As anticipated, GraHIL-based deep-red PhOLEDs showed better performance than did the deep-red PhOLEDs, where PEDOT:PSS was used as HIL (Table 2 and Table S3), due to the reduced injection barrier for the former one resulting in low V_{on} . For instance, the turn-on voltage (V_{on}) of the GraHIL-based deep-red PhOLEDs was about 4.2 V, while the V_{on} of the PEDOT:PSS-based deep-red PhOLEDs was in the range of 6.7-7.0 V (Fig. S8). Data of the deep-red PhOLEDs containing PEDOT:PSS are provided in Table S3. Fig. 2b and 2c shows the current density-voltage-luminance (J-V-L) and current efficiency-J-power efficiency (CE-J-PE) characteristics of the deep-red PhOLEDs using GraHIL. The CE and PE of the optimized deep-red PhOLED of TPQIr-HT were 15.87 cd/A and 5.05 lm/W, respectively, which were higher than those of CE (11.53 cd/A) and PE (4.26 lm/W) of TPQIr. Similarly, the deep-red PhOLED of TPQIr-HT exhibited a maximum EQE of 17.47%, compared to 13.70% for TPQIr (Fig. 3a). This is one of the best EQEs reported for solution-processed red/deep-red PhOLEDs (see Table S4, which summarizes the reported device performances). The high hole and electron mobility of TPQIr-HT relative to TPQIr resulted in good charge balance in EML, which enhanced the performance of TPQIr-HT in PhOLEDs. However, the

deep-red PhOLED of TPQIr-ET showed better performance (EQE: 21.48%) than did TPQIr-HT in the similar device structure. Mobility study revealed that TPQIr-ET-based deep-red PhOLED had better electron mobility than hole mobility, which was reversed from the case of the TPQIr-HT-based device. Actually, the mobility of electron-carriers is several orders of magnitude lower than that of hole-carriers in organic materials.⁴⁴ Therefore, the introduction of the ET group into the Ir(III) complex enhanced the mobility of the low mobile electron carriers, and thus balanced the injected charge carriers in the EML.

The orange PhOLEDs exhibited a similar trend to the deep-red PhOLEDs as shown in Table 3. The device configuration adopted in this study was ITO/PEDOT:PSS/TAPC:26DCzPPy:Ir(III) complex (10 wt%)/TmPyPB/LiF/Al, where TAPC:26DCzPPy acts as the mixed cohost for the EML. We also fabricated a control device using *m*-CF₃DPQIr as the dopant to compare the effect of mCP and OXD groups on device performance.

The J-V-L and CE-J-PE characteristics of the orange PhOLEDs doped with *m*-CF₃DPQIr-HT and *m*-CF₃DPQIr-ET are summarized in Fig. 2e and 2f. The CE and PE of the optimized orange PhOLEDs of *m*-CF₃DPQIr-HT and *m*-CF₃DPQIr-ET were 52.16 cd/A and 24.56 lm/W and 46.59 cd/A and 21.03 lm/W, respectively, which were higher than those of the CE (44.23 cd/A) and PE (19.85 lm/W) of *m*-CF₃DPQIr. Also, the orange PhOLEDs of *m*-CF₃DPQIr-HT and *m*-CF₃DPQIr-ET exhibited maximum EQEs of 21.61 and 18.39%, compared to 17.34% for *m*-CF₃DPQIr (Fig. 3d). This is one of the highest EQEs reported for solution-processed orange PhOLEDs (see Table S5, which summarizes the reported device performances). The improvement in performance of the orange PhOLEDs of *m*-CF₃DPQIr-HT and *m*-CF₃DPQIr-ET compared to the PhOLED of *m*-CF₃DPQIr was attributed to the good charge balance in EML.

In addition, good solubility and thin film formability of the EML materials are also important factors for the fabrication of high performance solution-processed PhOLEDs. Therefore, we analyzed the surface morphology of the EML films consisting of TPQIr, TPQIr-HT, TPQIr-ET, *m*-CF₃DPQIr, *m*-CF₃DPQIr-HT, and *m*-CF₃DPQIr-ET using atomic force microscopy (AFM). The root-mean-square (RMS) surface roughness values were 0.30, 0.34, 0.40, 0.41, 0.40, and 0.43 nm for TPQIr, TPQIr-HT, TPQIr-ET, *m*-CF₃DPQIr, *m*-CF₃DPQIr-HT, and *m*-CF₃DPQIr-ET, respectively (Fig. S9). This suggests that the thin film formability of TPQIr-HT and *m*-CF₃DPQIr-HT is better than that of TPQIr-ET and *m*-CF₃DPQIr-ET, respectively, in EML due to the better solubility of the carbazole (mCP) than the OXD moiety in chlorobenzene. The deep-red PhOLEDs, irrespective of the dopant, HIL and luminance range, exhibited the same electroluminescence (EL) peak at 624 nm (Fig. 3b) and the CIE coordinates of (0.67, 0.32) (Fig. 3c) representing the saturated deep-red emission, which is highly sought after for deep-blue emission.

The CIE coordinates and the efficiency of TPQIr-HT were better than our previously reported solution-processed PhOLEDs containing phenylquinoline-based deep-red emitting heteroleptic Ir(III) complexes such as *o*-LIrtmd,³⁰ (FPQ)₂Ir(pic-N-O)³¹ and (EO-CVz-PhQ)₂Ir(acac).³² Similarly, the orange PhOLEDs exhibited the same EL peak at 575 nm (Fig. 3e) and the same CIE coordinates of (0.54, 0.46) (Fig. 3f), irrespective of the dopant and luminance range.

4. Conclusion

In summary, we attached an mCP-based HT unit and an OXD-based ET unit to the heteroleptic Ir(III) complexes, TPQIr and *m*-CF₃DPQIr, to achieve a good charge balance in EML by improving the HT and ET properties of TPQIr-HT, *m*-CF₃DPQIr-HT and *m*-CF₃DPQIr-ET as compared with the parent Ir(III) complexes, TPQIr and *m*-CF₃DPQIr. As a

dopant, the new Ir(III) complex, TPQIr-HT, showed deep-red EL in solution-processed PhOLEDs. Introduction of the mCP moiety improved the carrier mobilities and device performance relative to TPQIr, without affecting the deep-red CIE coordinates (0.67, 0.32). We achieved a high EQE of 17.47% for the deep-red PhOLED of TPQIr-HT, which is superior to the performance of TPQIr (EQE: 13.70%). As dopants, the new Ir(III) complexes, *m*-CF₃DPQIr-HT and *m*-CF₃DPQIr-ET, also showed orange EL in solution-processed PhOLEDs. We achieved high EQEs of 21.64% and 18.39 % for the orange PhOLED of *m*-CF₃DPQIr-HT and *m*-CF₃DPQIr-ET, respectively, which is higher than that of *m*-CF₃DPQIr (EQE: 17.34%). The overall results of these PhOLEDs with multi-functional Ir(III) complexes show that the introduction of new functional units (HT/ET) is an effective method to improve the device performance.

Acknowledgment

W. Cho and G. Sarada contributed equally to this work. This work was supported by the Pioneer Research Center Program through the National Research Foundation of Korea funded by the Ministry of Science, ICT & Future Planning (MSIP) of Korea (NRF-2013M3C1A3065522).

References

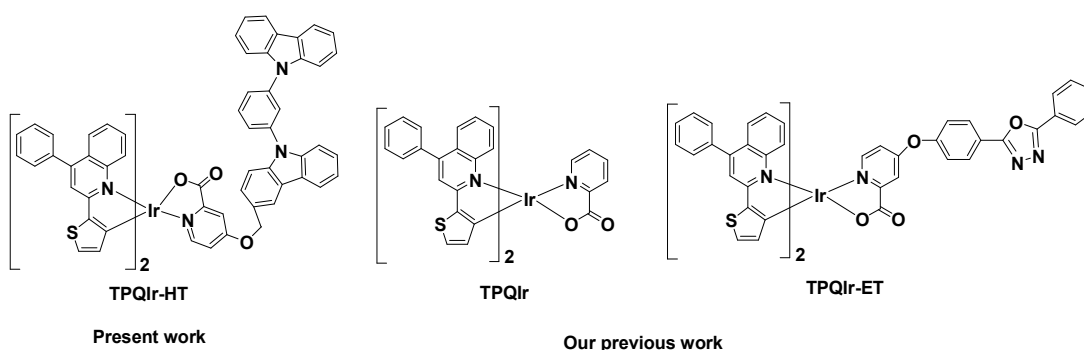
1. T. Qin, J. Ding, M. Baumgarten, L. Wang and K. Mullen, *Macromol. Rapid Commun.*, 2012, **33**, 1036.
2. C.-L. Ho, H. Li and W.-Y. Wong, *J. Organomet. Chem.*, 2014, **751**, 261.
3. X. Xu, X. Yang, J. Zhao, G. Zhou and W.-Y. Wong, *Asian J. Org. Chem.* 2015, **4**, 394.

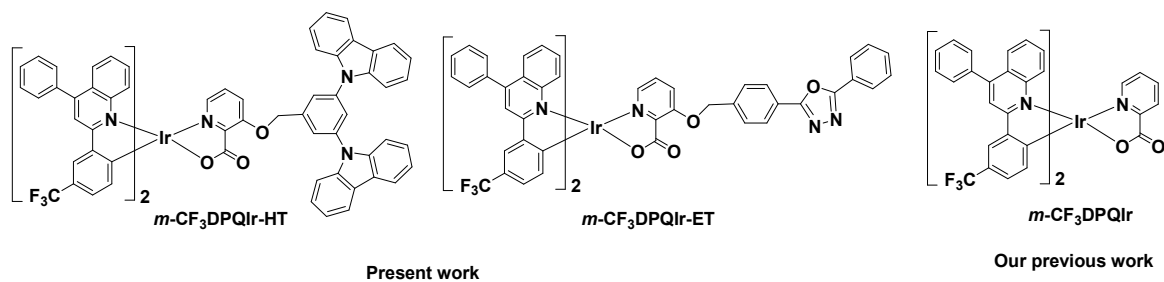
4. X. Dai, Z. Zhang, Y. Jin, Y. Niu, H. Cao, X. Liang, L. Chen, J. Wang and X. Peng, *Nature*, 2014, 515, 96.
5. J. Ding, J. Lu, Y. Cheng, Z. Xie, L. Wang, X. Jing and F. Wang, *Adv. Funct. Mater.*, 2008, **18**, 2754.
6. Y. You, S. Y. Park, *Dalton Trans.*, 2009, 1267.
7. G. J. Hedley, A. Ruseckas, I. D.W. Samuel, *Chem. Phys. Lett.*, 2008, **450**, 292.
8. R. Wang, D. Liu, R. Zhang, L. Deng and J. Li, *J. Mater. Chem.*, 2012, **22**, 1411.
9. Y.-L. Deng, L.-S. Cui, Y. Liu, Z.-K. Wang, Z.-Q. Jiang and L.-S. Liao, *J. Mater. Chem. C*, 2016, **4**, 1250.
10. S. Cao, L. Hao, W.-Y. Lai, H. Zhang, Z. Yu, X. Zhang, X. Liu and W. Huang, *J. Mater. Chem. C*, 2016, DOI: 10.1039/c6tc00856a.
11. M. Zhu, Y. Li, S. Hu, C. Li, C. Yang, H. Wu, J. Qin and Y. Cao, *Chem. Commun.*, 2012, **48**, 2695.
12. B. Jiang, Y. Gu, J. Qin, X. Ning, S. Gong, G. Xie and C. Yang, *J. Mater. Chem. C*, 2016, **4**, 3492.
13. X. Liu, B. Yao, Z. Zhang, X. Zhao, B. Zhang, W.-Y. Wong, Y. Cheng and Z. Xie, *J. Mater. Chem. C*, 2016, **4**, 5787.
14. G. Li, Y. Feng, T. Peng, K. Ye, Y. Liu and Y. Wang, *J. Mater. Chem. C*, 2015, **3**, 1452.
15. G. Li, D. Zhu, T. Peng, Y. Liu, Y. Wang and M. R. Bryce, *Adv. Funct. Mater.*, 2014, **24**, 7420.
16. R. Wang, D. Liu, H. Ren, T. Zhang, H. Yin, G. Liu and J. Li, *Adv. Mater.*, 2011, **23**, 2823.
17. H.-H. Chou, Y.-K. Li, Y.-H. Chen, C.-C. Chang, C.-Y. Liao and C.-H. Cheng, *ACS*

- Appl. Mater. Interfaces*, 2013, **5**, 6168.
18. H. Fukagawa, T. Shimizu, H. Hanashima, Y. Osada, M. Suzuki, H. Fujikake, *Adv. Mater.*, 2012, **24**, 5099.
19. K.-H. Kim, J.-L. Liao, S. W. Lee, B. Sim, C.-K. Moon, G.-H. Lee, H. J. Kim, Y. Chi, J.-J. Kim, *Adv. Mater.*, 2016, **28**, 2526.
20. M.-C. Tang, C. K.-M. Chan, D. P.-K. Tsang, Y.-C. Wong, M. M.-Y. Chan, K. M.-C. Wong and V. W.-W. Yam, *Chem. Eur. J*, 2014, **20**, 15233.
21. X. Yang, X. Xu, J. Zhao, J. Dang, Z. Huang, X. Yan, G. Zhou and D. Wang, *Inorg. Chem.*, 2014, **53**, 12986.
22. H. J. Bae, J. Chung, H. Kim, J. Park, K. M. Lee, T.-W. Koh, Y. S. Lee, S. Yoo, Y. Do and M. H. Lee, *Inorg. Chem.*, 2014, **53**, 128.
23. S. Reineke, F. Lindner, G. Schwartz, N. Seidler, K. Watzler, B. Lussem and K. Leo, *Nature*, 2009, **459**, 234.
24. C. Fan, L. Zhu, B. Jiang, Y. Li, F. Zhao, D. Ma, J. Qin and C. Yang, *J. Phys. Chem. C*, 2013, **117**, 19134.
25. C.-C. Chen, H.-Y. Lin, C.-H. Li, J.-H. Wu, Z.-Y. Yu, L.-L. Lee, M.-S. Jeng, C.-C. Lin, J.-H. Jou and H.-C. Kuo, *Int. J. Photoenergy*, 2014, **6**, article ID 851371.
26. H. Wu, G. Zhou, J. Zou, C. -L. Ho, W. -Y. Wong, W. Yang, J. Peng and Y. Cao, *Adv. Mater.*, 2009, **21**, 4181.
27. B. Zhang, G. Tan, C. -S. Lam, B. Yao, C. -Lam. Ho, L. Liu, Z. Xie, W. -Y. Wong, J. Ding and L. Wang, *Adv. Mater.*, 2012, **24**, 1873.
28. M. Zhu, Y. Li, B. Jiang, S. Gong, H. Wu, J. Qin, Y. Cao and C. Yang, *Org. Electron.*, 2015, **26**, 400.
29. X. Liu, S. Wang, B. Yao, B. Zhang, C.-L. Ho, W.-Y. Wong, Y. Cheng and Z. Xie

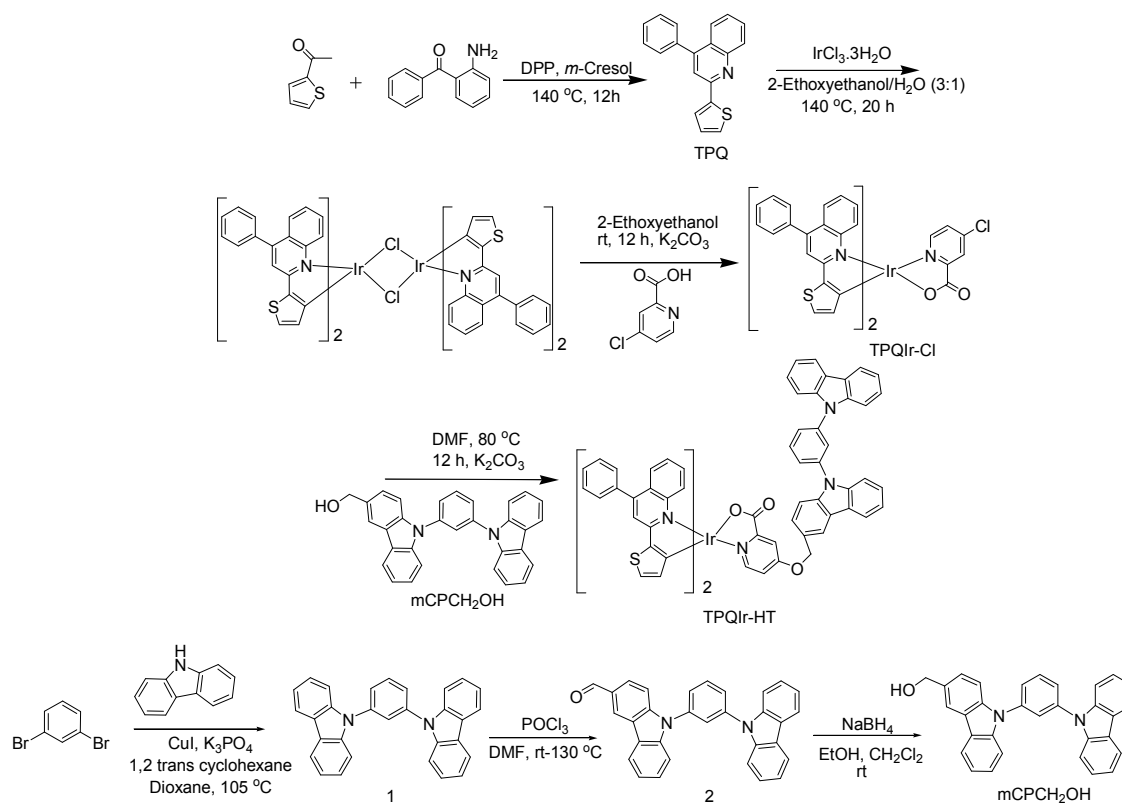
- Org. Electron.*, 2015, **21**, 1.
30. G. Sarada, J. Yoon, W. Cho, M. Cho, D. W. Cho, S. O. Kang, Y. Nam, J. Y. Lee and S.-H. Jin, *J. Mater. Chem. C*, 2016, **4**, 113.
31. J. Park, J. S. Park, Y. G. Park, J. Y. Lee, J. W. Kang, J. Liu, L. Dai and S.-H. Jin, *Org. Electron.*, 2013, **14**, 2114.
32. S.-J. Lee, J.-S. Park, M. Song, I. A. Shin, Y.-I. Kim, J. W. Lee, J.-W. Kang, Y.-S. Gal, S. Kang, J. Y. Lee, S.-H. Jung, H.-S. Kim, M.-Y. Chae and S.-H. Jin, *Adv. Funct. Mater.*, 2009, **19**, 2205.
33. T. Giridhar, T.-H. Han, W. Cho, C. Saravanan, T.-W. Lee and S.-H. Jin, *Chem. –Eur. J.*, 2014, **20**, 8260.
34. T. Giridhar, C. Saravanan, W. Cho, Y. G. Park, J. Y. Lee and S.-H. Jin, *Chem. Commun.*, 2014, **50**, 4000.
35. T.-H. Kwon, M. K. Kim, J. Kwon, D.-Y. Shin, S. J. Park, C.-L. Lee, J.-J. Kim and J.-I. Hong, *Chem. Mater.*, 2007, **19**, 3673.
36. Z. Si, J. Li, B. Li, F. Zhao, S. Liu and W. Li, *Inorg. Chem.*, 2007, **46**, 6155.
37. M. J. Frisch, et al., *Al, Gaussian 09, Revision A. 1*, Gaussian Inc, Wallingford, CT, 2009.
38. C. Yao, J. Li, J. Wang, X. Xu, R. Liu, L. Li, *J. Mater. Chem. C*, 2015, **3**, 8675.
39. C. -G. Zhen, Y. -F. Dai, W. -J. Zeng, Z. Ma, Z. -K. Chen, J. Kieffer, *Adv. Funct. Mater.*, 2011, **21**, 699.
40. J.-H. Jou, W.-B. Wang, S.-Z. Chen, J.-J. Shyue, M.-F. Hsu, C.-W. Lin, S.-M. Shen, C.-J. Wang, C.-P. Liu, C.-T. Chen, M.-F. Wu and S.-W. Liu, *J. Mater. Chem.*, 2010, **20**, 8411.
41. T. -W. Lee, Y. Chung, O. Kwon, J. -J. Park, *Adv. Funct. Mater.*, 2007, **17**, 390.

42. T. -H. Han, M. -R. Choi, S. -Y. Woo, S. -Y. Min, C. -L. Lee, T. -W. Lee, *Adv. Mater.*, 2012, **24**, 1487.
43. T. -H. Han, Y. Lee, M. -R. Choi, S. -H. Woo, S. -H. Bae, B. H. Hong, J. -H. Ahn, T. -W. Lee, *Nat. Photonics*, 2012, **6**, 105.
44. H. Yersin, *Highly efficient OLEDs with Phosphorescent Materials*, WILEY-VCH Verlag GmbH & Co., 2008, p. 395.

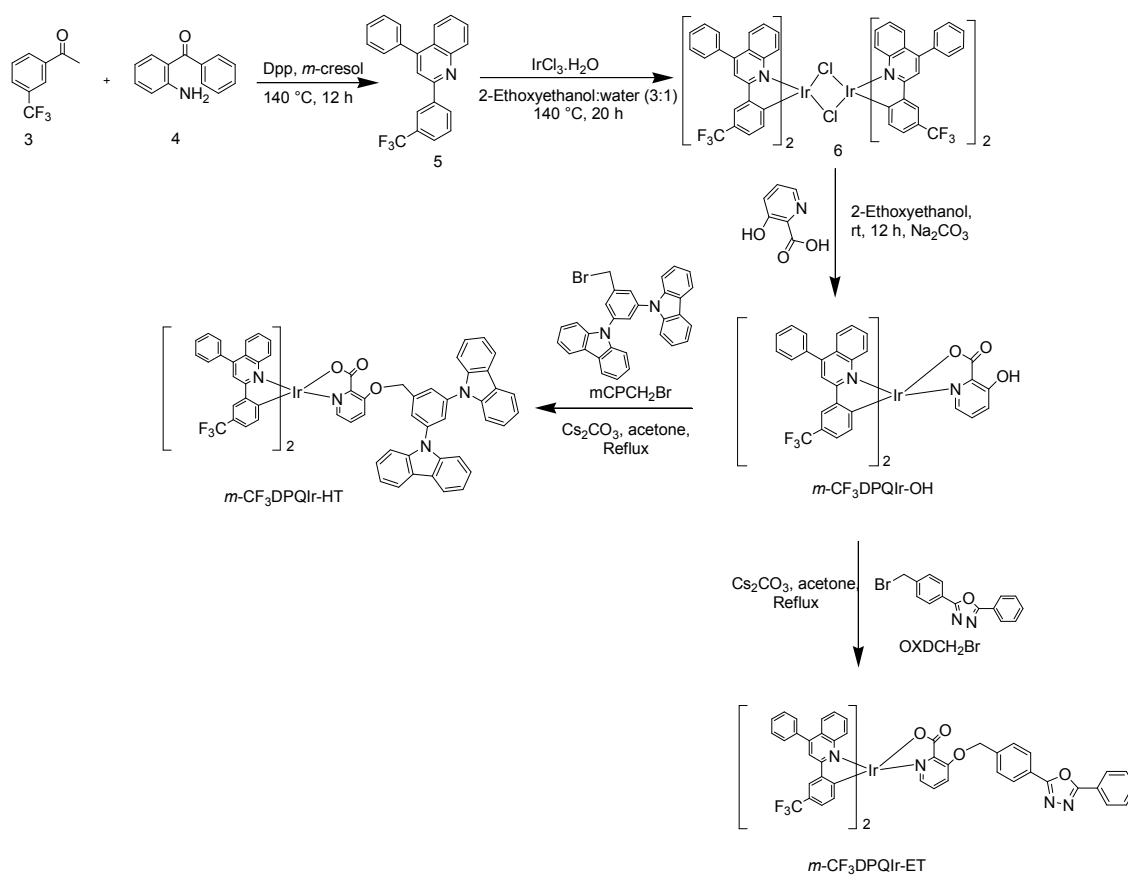




Scheme 1. Molecular structures of TPQIr-HT, TPQIr, TPQIr-ET, *m*-CF₃DPQIr-HT, *m*-CF₃DPQIr-ET, and *m*-CF₃DPQIr.



Scheme 2. Synthetic route of TPQIr-HT.



Scheme 3. Synthetic route of *m*-CF₃DPQIr-HT and *m*-CF₃DPQIr-ET.

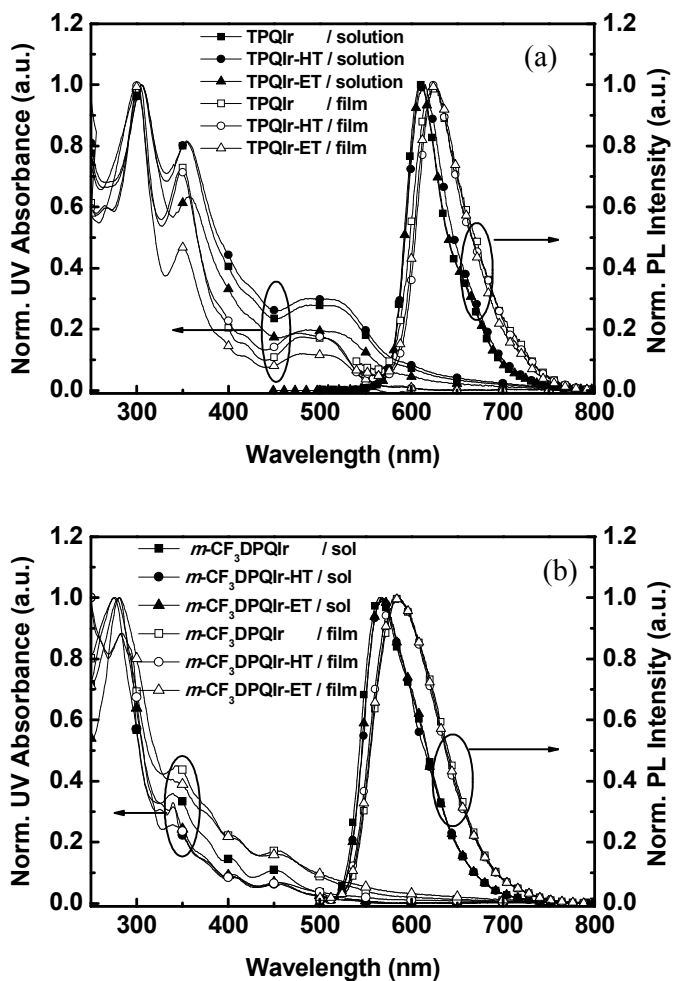


Fig. 1 (a) UV-visible absorption and PL spectra of TPQIr-HT in comparison with TPQIr and TPQIr-ET and (b) UV-visible absorption and PL spectra of *m*-CF₃DPQIr-HT, *m*-CF₃DPQIr-ET in comparison with *m*-CF₃DPQIr.

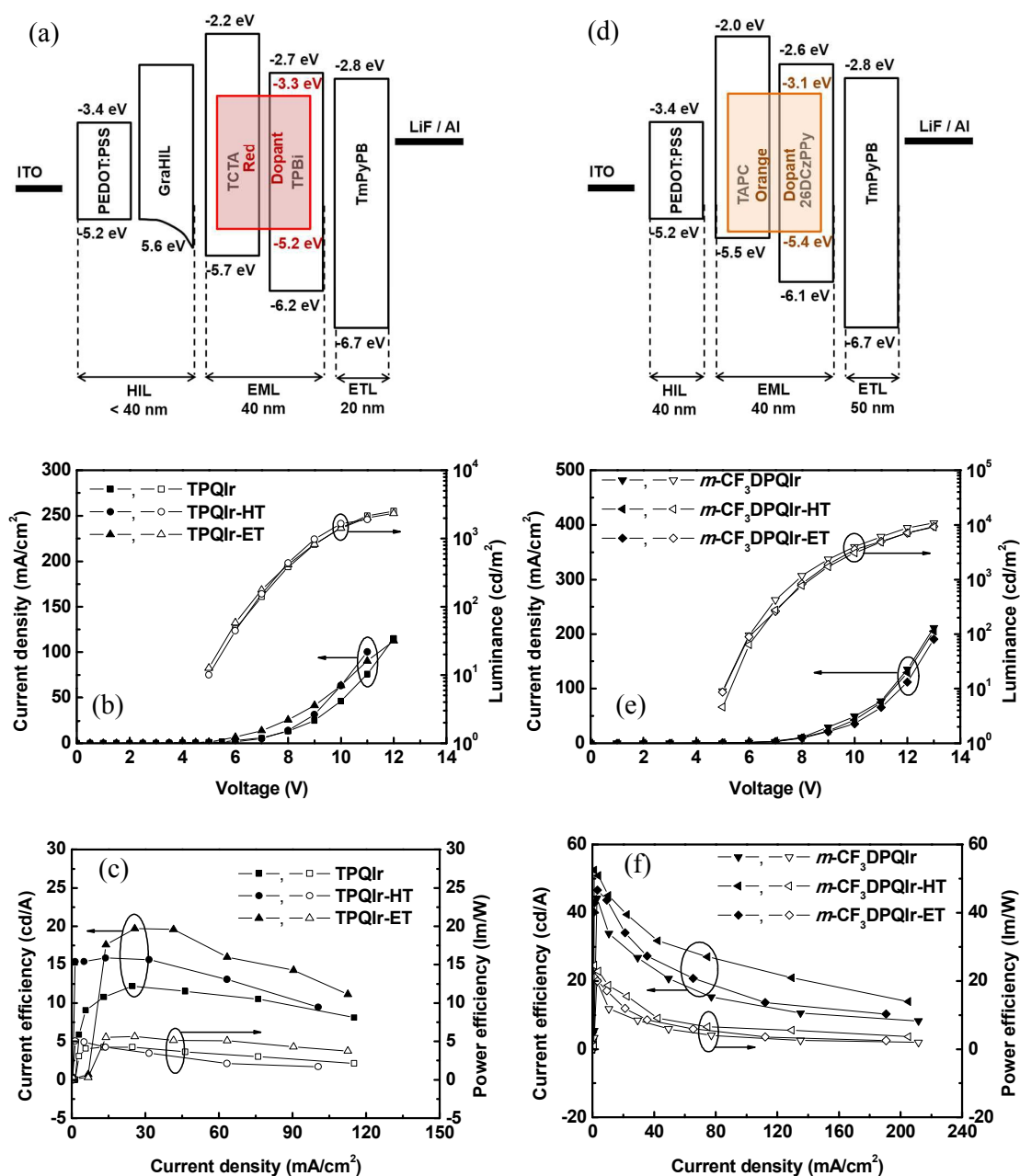


Fig. 2. (a) Energy level diagram, (b) J-V-L characteristics, and (c) CE-J-PE of TPQIr-HT in comparison with TPQIr and TPQIr-ET and (d) energy level diagram, (e) J-V-L characteristics, and (f) CE-J-PE of $m\text{-CF}_3\text{DPQIr}$ -HT and $m\text{-CF}_3\text{DPQIr}$ -ET in comparison with $m\text{-CF}_3\text{DPQIr}$.

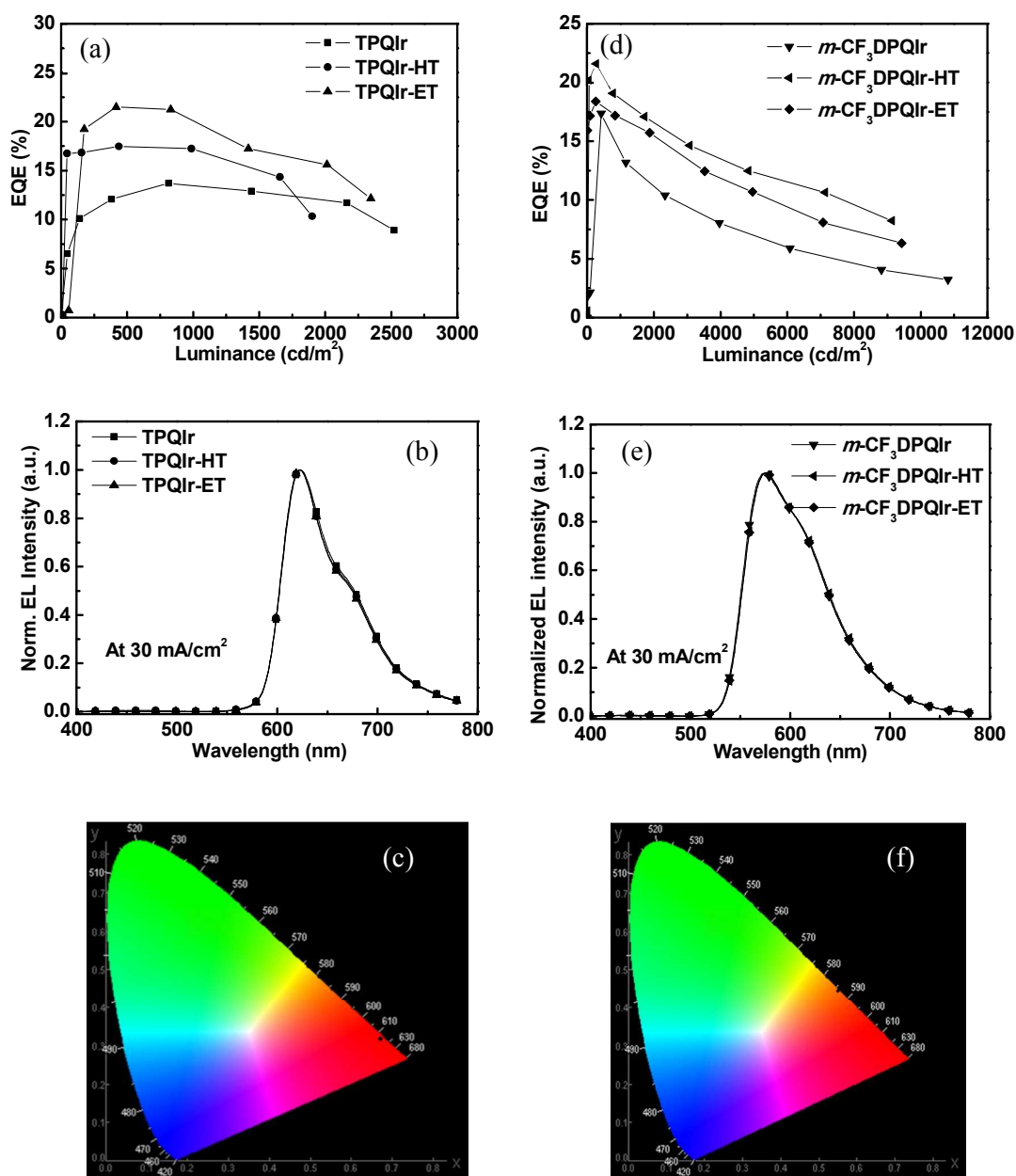


Fig. 3 (a) EQE vs. luminance, (b) EL spectra, and (c) CIE coordinates (at 30 mA/cm²) of TPQIr-HT in comparison with TPQIr and TPQIr-ET and (d) EQE vs. luminance, (e) EL spectra, and (f) CIE coordinates (at 30 mA/cm²) of *m*-CF₃DPQIr-HT and *m*-CF₃DPQIr-ET in comparison with *m*-CF₃DPQIr.

Table 1. Thermal, photophysical and electrochemical data of Ir(III) complexes.

Ir(III) complex	T _d ^a (°C)	λ _{abs} ^b (nm)	λ _{em} ^c (nm)	λ _{em} ^d (nm)	Φ _{PL} ^e (%)	HOMO/LUMO ^f (eV)	E _g ^g (eV)
TPQIr	338	302, 350, 480	610	625	0.22	-5.23/-3.24	1.95
TPQIr-HT	327	295, 344, 473	612	626	0.18	-5.24/-3.29	1.93
TPQIr-ET	350	299, 349, 480	610	625	0.20	-5.25/-3.27	1.96
<i>m</i> -CF ₃ DPQIr	362	274, 340, 455	566	583	0.65	-5.39/-3.11	2.13
<i>m</i> -CF ₃ DPQIr-HT	320	280, 339, 457	568	584	0.68	-5.41/-3.11	2.13
<i>m</i> -CF ₃ DPQIr-ET	321	281, 341, 453	567	583	0.66	-5.42/-3.10	2.14

^a Temperature with 5% mass loss measured by TGA with a heating rate of 10 °C/min under N₂. ^b Measured in CHCl₃ solution at 1.0 x 10⁻⁵ M concentration. ^c Maximum emission wavelength measured in CHCl₃ solution at 1.0 x 10⁻⁵ M concentration. ^d Maximum emission wavelength measured in a film state. ^e Measured in 1.0 x 10⁻⁵ M CHCl₃ solution relative to Ir(piq)₂(acac) (Φ_{PL} = 0.20) with 420 nm excitation. ^f Determined from the onset of CV oxidation and reduction calculated HOMO and LUMO level. ^g Optical band gap determined from the film state of UV-vis absorption edge value.

Table 2. Device performances of deep-red PhOLEDs with Ir(III) complexes.

Doping concentration (%)	Dopant	Turn on ^a (V)	EQE ^b (%)	CE ^b (cd/A)	PE ^b (lm/W)	Luminance ^b (cd/m ²)	CIE at 100 cd/m ² (x, y)
8	TPQIr	4.28	11.89	11.51	4.02	1907	(0.67, 0.32)
8	TPQIr-HT	4.31	14.20	14.04	4.41	1860	(0.67, 0.32)
8	TPQIr-ET	4.35	18.38	17.44	5.17	2092	(0.67, 0.32)
10	TPQIr	4.27	13.70	11.53	4.26	2521	(0.67, 0.32)
10	TPQIr-HT	4.28	17.47	15.87	5.05	1901	(0.67, 0.32)
10	TPQIr-ET	4.25	21.48	19.70	5.62	2345	(0.67, 0.32)
12	TPQIr	4.22	11.52	10.70	3.96	2422	(0.67, 0.32)
12	TPQIr-HT	4.34	14.51	13.68	4.60	2118	(0.67, 0.32)
12	TPQIr-ET	4.28	17.63	15.99	5.08	2355	(0.67, 0.32)

^a At 1 cd/m². ^b Maximum efficiency.

Table 3. Device performances of orange PhOLEDs with Ir(III) complexes.

Doping concentration (wt%)	Dopant	Turn on ^a (V)	EQE ^b (%)	CE ^b (cd/A)	PE ^b (lm/W)	Luminance ^b (cd/m ²)	CIE at 100 cd/m ² (x, y)
8	<i>m</i> -CF ₃ DPQIr	4.52	15.73	41.16	16.30	10015	(0.54, 0.46)
8	<i>m</i> -CF ₃ DPQIr-HT	4.58	17.52	44.89	18.85	9132	(0.54, 0.46)
8	<i>m</i> -CF ₃ DPQIr-ET	4.56	16.68	42.51	16.45	8780	(0.54, 0.46)
10	<i>m</i> -CF ₃ DPQIr	4.54	17.34	44.23	19.85	10820	(0.54, 0.46)
10	<i>m</i> -CF ₃ DPQIr-HT	4.63	21.64	52.16	24.56	9137	(0.54, 0.46)
10	<i>m</i> -CF ₃ DPQIr-ET	4.55	18.39	46.59	21.03	9427	(0.54, 0.46)
12	<i>m</i> -CF ₃ DPQIr	4.60	16.17	40.57	18.28	9464	(0.54, 0.46)
12	<i>m</i> -CF ₃ DPQIr-HT	4.69	19.53	48.36	22.79	8924	(0.54, 0.46)
12	<i>m</i> -CF ₃ DPQIr-ET	4.61	17.71	44.83	20.17	8890	(0.54, 0.46)

^a At 1 cd/m². ^b Maximum efficiency.